Analysis and optimization of a diffuse photon optical tomography of turbid media

David L. Everitt, Sung-po Wei, and X. D. Zhu*
Department of Physics, University of California at Davis, One Shields Avenue, Davis, California 95616-8677
(Received 28 June 1999; revised manuscript received 15 May 2000)

In a numerical study, we investigate a diffuse-photon computed tomography of a turbid medium. Using a perturbation approach, we relate through a matrix **K** a bulk heterogeneous distribution of the optical absorption coefficient μ_a that characterizes the heterogeneity in an otherwise homogeneous turbid medium to the diffuse photon flux that emerges from its surface. By studying the *condition number* ($\mathcal{N}_C$) of the matrix **K** as a function of illumination-detection schemes and choices of reconstruction grids, we explore strategies that optimize the fidelity and spatial resolution of the computed tomography.

PACS number(s): 02.60.Pn, 87.59.Fm

I. INTRODUCTION

In recent years, the optical computed tomography of a turbid medium based upon the measurement and analysis of the diffuse photon flux that emerges from the surface of the medium has drawn considerable research attention in the fields of optical physics and biomedical imaging [1–3]. This is motivated by the potential applications of such a nonintrusive tomographic imaging technique in breast cancer detection and other biomedical imaging [1–4]. To realize such a potential, one needs to address the issue of sensitivity, image contrast, image fidelity, and spatial and temporal resolutions. The last three are the primary subjects of this investigation.

A typical configuration of a diffuse-photon computed tomography is the following: one illuminates a turbid medium with a continuous-wave or amplitude-modulated light source and measures the transmitted or reflected diffuse photon flux that emerges from the surface of the medium. By establishing numerically the relation between the diffuse photon flux and the heterogeneity in the medium as characterized by the distribution of appropriate optical constants, one reconstructs the heterogeneity.

There are numerous reports of numerical and experimental studies of this subject in which a large variety of methodologies have been explored, and the quality of reconstructed images varies substantially [5–15]. Generally speaking, the reported illumination-detection schemes fall into two categories: one is of continuous wave, in which case the amplitude of the illuminating light source does not change in time [13–15]; the other is of alternating wave (i.e., ac or frequency domain), in which case the amplitude of the illuminating light source is modulated at a frequency in the range of 10^7 Hz, and both the amplitude and phase lag of the alternating part of the diffuse photon density or flux are measured [5–12]. The analysis methodologies also fall into two categories: one involves nonperturbation approaches such that the effect of the heterogeneity in a turbid medium on the diffuse photon distribution is treated exactly in essence by solving the diffusion equation with a *finite-difference* [11] or *finite-element* technique [12]; the other involves perturbation approaches where the effect of the heterogeneity is treated perturbatively [7,8,13,14,16–18]. The latter are suitable for potential applications in *early* breast cancer detection. There are other advantages that we will get to very shortly. Despite these extensive efforts, there has been no *systematic* evaluation of the overall performance or the ''cost and benefit'' of various illumination-detection schemes and choices of reconstruction grids. An important question to ask is, given the precision and accuracy of the diffuse photon flux measurement and the model description, what is the achievable image quality (in terms of sensitivity, contrast, fidelity, and spatial and temporal resolution)? The present paper is an effort toward such a systematic analysis.

We report a numerical study of a diffuse-photon computed tomography with a continuous-wave (cw) illumination-detection scheme. The cw scheme is advantageous as it enables simultaneous measurements of the diffuse photon flux at a large number of surface positions and reduces the measurement error close to the statistical photon counting limit. For the analysis, we adopt a perturbation approach [7,14]. It has the following advantages: (1) it *linearly* relates the variation in the diffuse photon density or the flux emerging from the surface through a matrix **K** to the optical absorption coefficients of the interrogated heterogeneity in a turbid medium, and as a result, the computational procedure and optimization of image reconstruction are straightforward; (2) it renders the image reconstruction simply a form of an inversion of the matrix **K** multiplied by a set of flux values; (3) it provides a *convenient* and *effective* means to assess the mutual independence or sufficiency of a set of flux measurements for image reconstruction and in turn enables the optimization of the illumination-detection schemes and the choices of reconstruction grids.

The essence of our study is a systematic analysis of the matrix **K**. Since the diffusion description of diffuse photons has a limited numerical accuracy and diffuse photon flux measurements have finite precision and accuracy, the quality of the reconstructed image is subject to these errors. The effect of these errors is determined by the conditioning of the matrix **K**. Through a standard singular value decomposition, **K** can be expressed as a product of three matrices, $\mathbf{K}=\mathbf{U}\mathbf{W}\mathbf{V}^{-1}$, where **U** and **V** are two orthogonal matrices and **W** is a positive-definite diagonal matrix [19,20]. According to Golub and Van Loan, the relative error in the reconstructed image is proportional to those in the flux measure-

*Electronic address: xdzhu@physics.ucdavis.edu

ments and in the model approximation (including the numerical computation), and the proportionality constant equals the ratio of the largest to the smallest diagonal elements of **W** [21]. This ratio is defined as the *condition number* ($\mathcal{N}_C$) of **K**.

Using the condition number of **K** as the measure, we investigate (1) the optimal number of diffuse photon flux measurements beyond which one obtains no new information to improve the image reconstruction, (2) the relative effectiveness of different illumination-detection schemes, (3) the limitation on the achievable spatial resolution, and (4) the optimization of the choices of reconstruction grids. Using a particular illumination-detection scheme and a reconstruction algorithm, we demonstrate numerically the feasibility to achieve a spatial resolution of 2.4 mm when reconstructing objects in a 6 cm×6 cm×6 cm volume. We have achieved such a resolution using experimental data very recently [22]. Finally, we remark on the issue of the uniqueness of the reconstructed images as sought in the present work and in the works of others.

II. PERTURBATION METHOD OF A DIFFUSE-PHOTON COMPUTED TOMOGRAPHY

A. Perturbation treatment

For the purpose of this study, we assume that a turbid medium of interest is strongly scattering and yet nonabsorbing except for regions where the heterogeneity is located. The absorbing heterogeneity or the objects of interest are characterized by a distribution of the optical absorption coefficient $\mu_a(\mathbf{r})$ in the medium. The medium is illuminated with a suitable arrangement that will be specified shortly. We use the diffusion approximation of radiative transport theory [23] to establish the diffuse photon density $\Phi(\mathbf{r})$ in the medium and the relation between the emerging diffuse photon flux $\mathbf{J}(\mathbf{r})$ at the surface of the medium and $\mu_a(\mathbf{r})$. Specifically, we assume that $\Phi(\mathbf{r})$ in the interior of the medium satisfies the diffusion equation and a set of appropriate boundary conditions. We treat the effect of $\mu_a(\mathbf{r})$ on $\Phi(\mathbf{r})$ and on $\mathbf{J}(\mathbf{r})$ as a perturbation. Let $\mathbf{J}_0(\mathbf{r})$ be the flux at the surface in the absence of the absorbing objects. We define the flux perturbation $\mathbf{j}(\mathbf{r})$ as the change in the flux caused by $\mu_a(\mathbf{r})$. The total flux is then given by

$$\mathbf{J}(\mathbf{r})=\mathbf{J}_0(\mathbf{r})+\mathbf{j}(\mathbf{r}). \tag{1}$$

In our numerical calculation, we consider a square turbid medium in two dimensions with a side equal to L. One side is illuminated with a continuous-wave light $I_{\rm inc}$ (*number of photons per second per unit length*). We measure the normal component of the diffuse photon flux that emerges from the opposite side. Objects of interest in the medium are characterized by a spatially varying optical absorption coefficient $\mu_a(\mathbf{r})\equiv\mu_a(x,y)$. The illumination-detection arrangement is illustrated in Fig. 1. The diffuse photon density $\Phi(\mathbf{r})=\Phi(x,y)$ within the medium is expressed as $\Phi(x,y)=\Phi_0(x,y)+\phi(x,y)$. Here $\Phi_0(x,y)$ is the unperturbed density in the absence of the objects and $\phi(x,y)$ is the perturbation caused by the objects. In steady state, we have

$$\boldsymbol{\nabla}\cdot[\mathbf{J}_0(x,y)+\mathbf{j}(x,y)]+v\,\mu_a(x,y)[\Phi_0(x,y)+\phi(x,y)]=0. \tag{2}$$

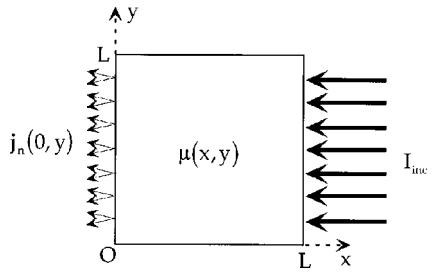

FIG. 1. Sketch of an illumination-detection arrangement for a diffuse-photon-computed tomography of a two-dimensional square turbid medium. One side of the medium is uniformly illuminated with a continuous-wave light. The normal component of the diffuse photon flux j_n that emerges from the opposite side is detected with an imaging optics (not shown).

Here $v=c/\bar{n}$ is the mean velocity of the diffuse photons in between scattering events and $\bar{n}$ is the average index of refraction of the medium. In addition, $\mathbf{J}(\mathbf{r})$ and $\Phi(x,y)$ satisfy Fick's law

$$\mathbf{J}_0(x,y)+\mathbf{j}(x,y)=-D\boldsymbol{\nabla}[\Phi_0(x,y)+\phi(x,y)], \tag{3}$$

with $D=(1/3)v\,l_{\rm tr}$ being the diffusion constant for the photons inside the medium. $l_{\rm tr}\equiv 1/\mu_s'$ is the reduced scattering or transport mean free path. μ_s' is the reduced scattering coefficient. The lowest-order perturbation to $\Phi_0(x,y)$ is given by

$$\phi(x,y)=-\frac{v}{D}\int\int dx'dy'\Phi_0(x',y')\times G(x,y;x',y')\mu_a(x',y'). \tag{4}$$

Here $G(x,y;x',y')$ is the Green function for the two-dimensional Laplacian operator $\nabla^2=\partial^2/\partial x^2+\partial^2/\partial y^2$ with vanishing boundary conditions. For example, let the side at $x=L$ be uniformly illuminated as shown in Fig. 1. The unperturbed diffuse photon density $\Phi_0(x,y)$ satisfies the boundary conditions $\Phi_0(x=L,y)=I_{\rm inc}l_{\rm tr}/D$ and $\Phi_0(x,y)=0$ at the other three sides. The normal component of the diffuse photon flux perturbation emerging from the opposite side at $x=0$,

$$j_n(x=0,y)=-\int_0^L dx'\int_0^L dy'\,v\,\Phi_0(x',y')\times\frac{\partial G(x=0,y;x',y')}{\partial x}\mu_a(x',y'), \tag{5}$$

forms one set of diffuse photon flux data. We can similarly obtain three additional sets of flux data by sequentially illuminating each of the other three sides and measuring the flux emerging from its opposite side. We reconstruct the objects by calculating $\mu_a(\mathbf{r}')$ from the flux perturbation data j_n [7,14]. For image reconstruction our present illumination-detection scheme is *sufficient* and *effective* when all four sets of the flux data are used. The four flux data sets j_n as a function the optical absorption coefficients $\mu_a(\mathbf{r}')$ can be combined into by a single integral equation

$$j_n(\mathbf{r}_s)=\int_0^L dx'\int_0^L dy'K(\mathbf{r}_s;\mathbf{r}')\mu_a(\mathbf{r}'). \tag{6}$$

We use $\mathbf{r}_s$ to represent the coordinates along the edge of the medium and $\mathbf{r}'$ to represent the interior coordinates. The kernel function $K(\mathbf{r}_s;\mathbf{r}')$ varies depending upon on which side of the medium the flux $j_n(\mathbf{r}_s)$ is detected.

B. Matrix equation

The numerical analysis of $K(\mathbf{r}_s;\mathbf{r}')$ is at the heart of the present work. Usually, $K(\mathbf{r}_s;\mathbf{r}')$ is in a form that does not afford an analytical transformation that *directly* solves for $\mu_a(\mathbf{r}')$. One resorts to a numerical solution where the distributions of both $\mu_a(\mathbf{r}')$ and $j_n(\mathbf{r}_s)$ are represented by discrete sets of numbers. In our case the medium is represented by N discrete pixels. The centers of these pixels form, for example, a square lattice as an image reconstruction grid. $j_n(\mathbf{r}_s)$ are measured at selected M points along the edge of the medium. As a result, Eq. (6) is reduced to a matrix equation

$$(j_n)_p=\sum_{q=1}^{N} K_{pq}(\mu_a)_q \tag{7a}$$

or, in matrix equation form,

$$\tilde{j}_n=\mathbf{K}\tilde{\mu}_a, \tag{7b}$$

with $P=1,2,\ldots,M$. Here $(\mu_a)_q$ is the optical absorption coefficient at the center of the qth pixel. $(j_n)_p$ is the normal component of the flux emerging at the pth point $(\mathbf{r}_s)_p$ along the edge. K_{pq} is the product of $K((\mathbf{r}_s)_p;\mathbf{r}')$ with an appropriate area element $\Delta x\,\Delta y$. Since the matrix $\mathbf{K}$ in Eq. (7b) is of order $M\times N$ and is usually not a square matrix (as will be clear shortly), solving Eq. (7b) for $\tilde{\mu}_a$ can be done by the standard method of *singular value decomposition* (SVD) of $\mathbf{K}$ [19,20]. As described by Press *et al.* [20], a rectangular matrix $\mathbf{K}$ can be decomposed into a product of a column-orthogonal matrix $\mathbf{U}$ of order $M\times N$, a positive-definite diagonal matrix $\mathbf{W}$ of order $N\times N$, and the inverse of an orthogonal matrix $\mathbf{V}$ of order $N\times N$, namely, $\mathbf{K}=\mathbf{U}\mathbf{W}\mathbf{V}^{-1}$. From Eq. (7b) or $\tilde{j}_n=\mathbf{U}\mathbf{W}\mathbf{V}^{-1}\tilde{\mu}_a$, we find

$$\tilde{\mu}_a=\mathbf{V}\mathbf{W}^{-1}\mathbf{U}^{-1}\tilde{j}_n. \tag{8}$$

C. Sensitivity of $\tilde{\mu}_a$ to variations in K and $\tilde{j}_n$

It is well known that Eq. (6) has the form of a Fredholm integral equation of the first kind where the kernel function $K(\mathbf{r}_s;\mathbf{r}')$ is strongly smoothing [24]. As a result, large changes in $\tilde{\mu}_a$ are mapped into small changes in $\tilde{j}_n$ and consequently small uncertainties in $\tilde{j}_n$ and numerical errors in $\mathbf{K}$ produce large variations in $\tilde{\mu}_a$ upon inversion. In other words, the matrix $\mathbf{K}$ is ill conditioned [20]. The large sensitivity of the reconstructed $\tilde{\mu}_a$ to the errors in $\tilde{j}_n$ and $\mathbf{K}$ reflects on the insufficiency of the flux measurements for fully characterizing the heterogeneity in the interior of a turbid medium.

Since both $\mathbf{U}$ and $\mathbf{V}$ are orthogonal matrices, the ill conditioning of $\mathbf{K}$ is characterized by the diagonal matrix $\mathbf{W}$. Golub and van Loan showed that the upper limit of the relative change in the norm of $\tilde{\mu}_a$ is proportional to the sum of the relative variations in the norms of $\mathbf{K}$ and $\tilde{j}_n$ with the proportionality constant equal to the ratio of the largest to the smallest diagonal element in $\mathbf{W}$ [21]. Let $\sigma_1,\sigma_2,\ldots,\sigma_N$ be the diagonal elements of $\mathbf{W}$ in decreasing order. They are called the singular values of matrix $\mathbf{K}$. The ratio of σ_1 to σ_N is defined as the condition number or $\mathcal{N}_C$ of matrix $\mathbf{K}$ [21],

$$\mathcal{N}_C\equiv\sigma_1/\sigma_N. \tag{9}$$

The $\mathcal{N}_C$ of $\mathbf{K}$ is thus the parameter that characterizes the sensitivity of the reconstructed $\tilde{\mu}_a$ to the variations in $\mathbf{K}$ and $\tilde{j}_n$. The variation in $\mathbf{K}$ comes from the model approximation, including the errors in the boundary conditions, the discretization of the original integral equation, and the actual numerical calculation. The variation in $\tilde{j}_n$ comes from the finite signal-to-noise ratio in the flux measurements.

The condition number $\mathcal{N}_C$ depends on choices of illumination-detection arrangements and reconstruction grids. Optimizing these choices to reduce the condition number and in turn to achieve the best image resolution is the goal of this paper.

It is noteworthy that the sensitivity of the image reconstruction to the errors in the data and in the computation is ubiquitous in all forms of diffuse-photon computed tomography. Such a sensitivity has not been analyzed systematically and quantitatively.

D. Regularization

Because of the high sensitivity to finite numerical precision and accuracy in $\mathbf{K}$ and in the measured flux j_n, a direct application of Eq. (8) usually yields images that are plagued by erroneous backgrounds, including artifacts. In reality, such a high sensitivity is contained by seeking an approximate solution to Eq. (7b) through, for example, the method of regularization [25,26]. The latter refers to making assumptions about the expected solution and introducing *additional* constraining parameters in the reconstruction that hopefully yields a reasonable, approximate solution. The SVD approach enables one to apply the regularization in a controlled and quantified way.

The process of regularization introduces a form of ''spatial'' filtering such that the contribution from small diagonal elements in the matrix $\mathbf{W}$ is reduced or eliminated. We use the zeroth-order regularization of Tikhonov [25,26], which defines a regularized solution $\tilde{\mu}_a^{(\alpha)}$ as that minimizes the functional

$$\alpha^2|\tilde{\mu}_a|^2+|\mathbf{K}^{(\alpha)}\tilde{\mu}_a-\tilde{j}_n|^2. \tag{10}$$

Here α is a positive constant. $\mathbf{W}^{(\alpha)}$ is a diagonal matrix of order $N\times N$ and its ith diagonal element is given by $\sigma_i(1+\alpha^2/\sigma_i^2)$. $\mu_a^{(\alpha)}$ is given by [27]

$$\tilde{\mu}_a^{(\alpha)}=\mathbf{V}(\mathbf{W}^{(\alpha)})^{-1}\mathbf{U}^{-1}\tilde{j}_n. \tag{11}$$

The solution $\tilde{\mu}_a^{(\alpha)}$ compromises between the smoothness and accuracy and approximates the original solution $\tilde{\mu}_a=\mathbf{V}\mathbf{W}^{-1}\mathbf{U}^{-1}\tilde{j}_n$. The smoothness is measured by the norm of the approximate solution $|\tilde{\mu}_a^{(\alpha)}|^2$ and weighted by the positive constant α^2. The accuracy is measured by the norm

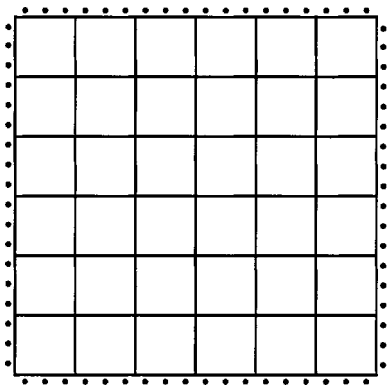

FIG. 2. Sketch of a square turbid medium that is uniformly discretized into $N=36$ pixels. The centers of the pixels form a 6×6 square lattice. The outgoing diffuse photon flux is detected at 18 uniformly distributed points from each side. There are a total of $M=18\times4=72$ flux measurement points.

of the residual defined as $|\mathbf{K}\tilde{\mu}_a^{(\alpha)}-\tilde{j}_n|^2$. Equation (11) effectively imposes upon the matrix $\mathbf{W}$ a low-pass filter by replacing σ_i with $\sigma_i(1+\alpha^2/\sigma_i^2)$. Upon inversion, such a filter smoothly cuts off the effects of those diagonal elements that are less than α. If α is much smaller than the smallest diagonal element σ_N, the regularized solution will be very close to the original solution. If α is close to or large than the largest element σ_1, the regularized solution no longer resembles the original solution. A regularized solution $\tilde{\mu}_a^{(\alpha)}$ has a reduced sensitivity to the uncertainties in the kernel and in the flux measurements at the expense of spatial resolution and fidelity of the reconstructed image.

E. Issues at hand

Given the precision and accuracy in the flux measurement and in the kernel, a sensible approach is to seek an optimal combination of an illumination-detection scheme and an image reconstruction grid that minimizes the condition number $\mathcal{N}_C$. Even if the regularization may be needed after all, α may be chosen as close as possible to σ_N of the optimized $\mathbf{W}$. In the following numerical calculation, we address the following questions based upon an analysis of the condition number.

(1) Given a reconstruction grid, is there an optimal number of flux perturbation measurements beyond which the quality of the image reconstruction is no longer improved?

(2) How do different illumination-detection schemes compare with one another?

(3) What is the limit on the spatial resolution in a diffuse-photon computed tomography?

(4) Can and how do we optimize the choices of image reconstruction grids to obtain the best overall spatial resolution?

III. DEPENDENCE OF $\mathcal{N}_C$ ON THE NUMBER OF FLUX MEASUREMENTS, ILLUMINATION-DETECTION SCHEMES, AND CHOICES OF RECONSTRUCTION GRIDS

Our numerical calculation is performed on a square turbid medium in two dimensions. In our coordinate system, the medium occupies a region defined by $0\leqslant x\leqslant L$ and $0\leqslant y\leqslant L$. As illustrated in Fig. 1, we illuminate one side of the medium uniformly and detect the flux that emerges from the opposite side. Specifically, let the side at $x=L$ be illuminated with an incident photon flux $I_{\rm inc}$. The unperturbed diffuse photon density inside the medium is given by

$$\Phi_0(x,y)=\left(\frac{I_{\rm inc}l_{\rm tr}}{D}\right)\sum_{m=1,3,5,\ldots}^{\infty}\frac{4\sin(m\pi y/L)\sinh(m\pi x/L)}{m\pi\sinh(m\pi)}, \tag{12}$$

and the Green function is given by

$$G(x,y;x',y')=\sum_{m=1}^{\infty}\frac{2\sin(m\pi y/L)\sin(m\pi y'/L)\sinh(m\pi x_</L)\sinh[m\pi(L-x_>)/L]}{m\pi\sinh(m\pi)}, \tag{13}$$

where $x_<(x_>)$ refers to the lesser (greater) of x and x'. Using Eq. (5), $\mu_a(x',y')$ is mapped onto the normal component of the diffuse photon flux perturbation $j_n(x=0,y)$ that emerges from the opposite side at $x=0$. We repeat the procedure for each of the other three sides and obtain three additional equations for $j_n(x=L,y)$, $j_n(x,y=0)$, and $j_n(x,y=L)$ as functions of $\mu_a(x',y')$.

To proceed with the numerical computation, we uniformly discretize the interior of the square turbid medium into $N=n\times n$ pixels. The centers of these pixels form a square-lattice reconstruction grid. The discrete set of the optical absorption coefficients $\tilde{\mu}_a$ at these grid points is to be computed from the diffuse photon flux perturbation measurements. Without *a priori* knowledge of $\mu_a(x',y')$, it is sensible to make use of the flux perturbation data taken at M points *uniformly* distributed along the sides of the medium. Our detection scheme and the image reconstruction grid are illustrated in Fig. 2 where optical absorption coefficients at centers of $N=36$ pixels are to be determined from the flux perturbation obtained at $M=72$ points uniformly along theedge of the medium. Using Eqs. (4)–(7) together with Eqs. (12) and (13), we compute the matrix $\mathbf{K}$ and the condition number [20,21].

A. Optimal number of flux perturbation measurements

We ask the following question: Is it best to use as many diffuse photon flux perturbation data as possible? This is important as for a given reconstruction grid using more flux data involves a longer data acquisition time and leads to a

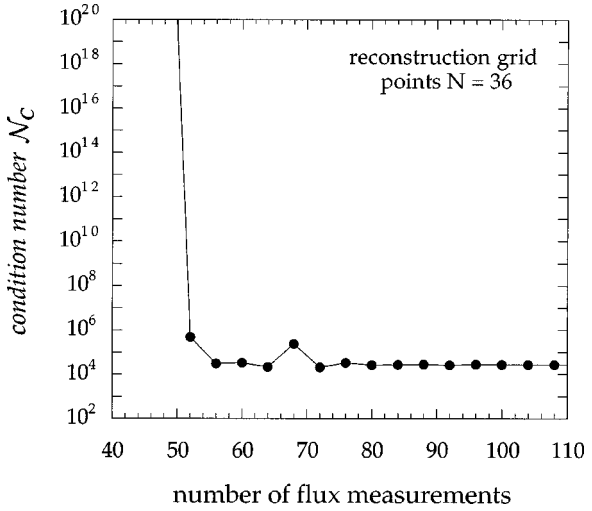

FIG. 3. Condition number $\mathcal{N}_C$ versus the number of diffuse photon flux perturbation measurements for a square-lattice reconstruction grid with 36 grid points as shown in Fig. 2. The flux measurements are made at points evenly distributed along the four sides of the square turbid medium.

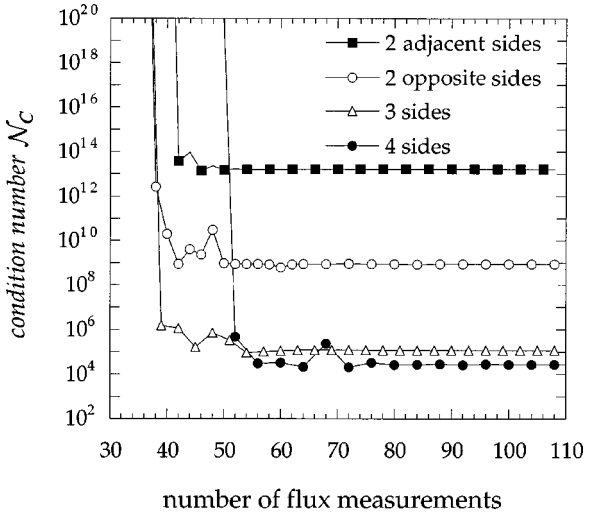

FIG. 4. Condition number $\mathcal{N}_C$ versus the number of diffuse photon flux perturbation data as illustrated in Fig. 2. Solid squares: the data taken from the measurements made on two adjacent sides, with one-half of the measurements from each side. Open circles: the data taken from the measurements made on two opposite sides, with one-half of the measurements from each side. Open triangles: the data taken from the measurements made on three sides, with one-third of the measurements from each side. Solid circles: the data taken from the measurements made on all four sides, with one-quarter of the measurements from each side.

larger matrix **K** that takes a longer time to compute. It would be undesirable in real-time imaging applications. Given a reconstruction grid and errors in the matrix computation and in the flux perturbation measurements, whether the quality or the signal-to-noise ratio of the reconstructed $\tilde{\mu}_a$ is improved by increasing the number of the flux measurements is determined by whether $\mathcal{N}_C$ is further reduced.

In Fig. 3, we display $\mathcal{N}_C$ versus the number of the flux perturbation measurements for $N=36$ reconstruction grid points. The data are taken from all four sides. We first find that if the number of measurements, M, equals the number of reconstruction grid points, N, then $\mathcal{N}_C$ is prohibitively large, indicating that the matrix **K** is indeed badly conditioned so that N flux perturbation measurements are grossly insufficient to reconstruct N optical absorption coefficients. $\mathcal{N}_C$ sharply decreases and levels off to an asymptotic value when the number of the flux measurements M is roughly *twice* that of the reconstruction grid points N. $\mathcal{N}_C$ no longer changes significantly when $M \geqslant 2N$. We have performed the calculations for $N=16$, 25, 49, and 144; the findings remain the same: (i) $\mathcal{N}_C$ is prohibitively large for $M \cong N$, and (ii) $\mathcal{N}_C$ sharply levels off for $M \geqslant 2N$. Our calculations for three dimensions indicate that the sufficiency of $M \sim 2N$ measurements is also a good rule.

This result indicates that for a given reconstruction grid there exists an optimal number of diffuse photon flux perturbation measurements beyond which one can no longer improve the quality of the image. For a uniform reconstruction grid with N grid points, the optimal number M_{opt} of flux measurements is roughly twice the number of the grid points, or $M_{\text{opt}} \approx 2N$. This is most important in applications where real-time imaging is desired. Excessive measurements do not improve the quality of the image and yet can drastically lengthen the image acquisition and processing time. Even in cases when the image acquisition time is not a limiting factor, one is better off improving the precision of the flux measurements and the accuracy of the model than increasing the number of the flux measurements.

B. Benefit of multiple illumination-detection arrangements

There have been numerous studies of diffuse-photon computed tomography where various source-detector configurations or illumination-detection arrangements were used [6,11,12,14]. We show that the optimization of illumination-detection arrangements can be made quantitatively through the evaluation of $\mathcal{N}_C$.

Our analysis is again performed on a square turbid medium as illustrated in Fig. 1. The medium is uniformly discretized into $N=6\times6=36$ pixels as illustrated in Fig. 2. We study the following illumination-detection arrangement: one side of the medium is uniformly illuminated, and the outgoing diffuse photon flux is measured on the opposite side, as shown in Fig. 1. By repeating the procedure for each of the other three sides, we arrive at four sets of flux perturbation data. We ask the following questions: (1) Will $\mathcal{N}_C$ settle to an asymptotic value if fewer than all four sets are used? (2) How does the asymptotic $\mathcal{N}_C$ change when more data sets are used rather than more data from the same set(s)?

In Fig. 4, we display $\mathcal{N}_C$ as a function of the number of the flux measurements with the data taken from (a) two adjacent sides, (b) two opposite sides, (c) three sides, on (d) all four sides. We find that $\mathcal{N}_C$ always reaches an asymptotic value when the number of the flux perturbation measurements exceeds twice the number of the reconstruction grid points, regardless of whether the data are taken from just one, two, three, or all four sets. If we use the flux perturbation data from only one side, $\mathcal{N}_C$ settles down to an extremely large number, 10^{40}. The asymptotic $\mathcal{N}_C$ improves dramatically when we use the data from more than one side. When we use the data taken from two sides that are adjacent to each other, the asymptotic $\mathcal{N}_C$ is reduced from 10^{40} to 10^{13}, by 27 orders of magnitude. By using the data from two

sides that are opposite to each other, the asymptotic $\mathcal{N}_C$ is reduced from 10^{40} to 10^9 by 31 orders of magnitude. If we use the flux data taken from three sides, $\mathcal{N}_C$ is reduced further from 10^9 to 10^5. If we use the data from all four sides, $\mathcal{N}_C$ drops to 3×10^4.

These findings underlie an early report by den Outer and co-workers and the experimental work by ourselves [13,15]. These authors studied the transmitted diffuse photons through a slab of a homogeneous turbid medium with a pointlike absorbing object embedded inside. They found that the diffuse photon flux perturbation that emerges from a surface shows the ''shadow'' of the object. The shadow becomes sharper and better defined as the object is brought close to the surface. As the object is moved away from the surface, the shadow quickly becomes blurred, although the center position of the shadow parallel to the surface plane vaguely reproduces that of the pointlike object. When using the flux perturbation data to reconstruct the position of the object, these authors found that (1) the location of the object parallel to the surface plane could be reproduced fairly well; (2) however, the depth position of the object normal to the surface plane is reproduced reasonably well *only* when the object is *very* close to the surface and poorly when the object is away from the surface.

The findings of these authors was a manifestation of the insufficiency of the flux data taken from only one surface to reconstruct the coordinates of the object. Similarly, in our present simulation of a square turbid medium in two dimensions, the insufficiency of the flux perturbation data from only one side is quantitatively represented by an extremely large $\mathcal{N}_C$. By taking the flux perturbation data from the two opposite sides, the depth position near both sides is better determined and correspondingly $\mathcal{N}_C$ drops from 10^{40} to 10^9.

From the first findings of these authors, it is clear that when the flux perturbation measurements from two adjacent sides are used, the information to reconstruct both the x and y coordinates of objects in our simulation should be more or less sufficient. This is quantitatively manifested by the dramatic decrease in $\mathcal{N}_C$ from 10^{40} to 10^{13}. When we use the data from three sides or all four sides, the information is further improved for image reconstruction of all regions in a square turbid medium. This is manifested by a further reduction of $\mathcal{N}_C$ down to 3×10^4.

At this point, it seems operationally simple to illuminate just one side and measure the flux perturbation from the other three sides. The drawback is that the diffuse photon flux emerging from the two sides that are adjacent to the illuminated side varies in strength over orders of magnitude. It is difficult to operate detectors with a large enough dynamic range at both ends to ensure a uniformly high signal-to-noise ratio in the flux perturbation measurements.

The result displayed in Fig. 4 in essence applies to other geometries of turbid media. Such a systematic analysis is essential in assessing the effectiveness and efficiency of different source-detector combinations or illumination-detection arrangements.

C. Dependence of $\mathcal{N}_C$ on the prescribed spatial resolution or the number of reconstruction grid points

Once the illumination-detection arrangement is optimized, the asymptotic $\mathcal{N}_C$ varies only with the choice of reconstruction grids. One of the important questions to ask is, what is the limit of the image resolution given an acceptable signal-to-noise ratio of the image field? In other words, what determines the density limit of the image reconstruction grid given an interrogated volume of a turbid medium? Assuming that the errors in the flux measurement and in **K** are already minimized, the achievable grid point density is determined only by $\mathcal{N}_C$.

In Fig. 5(a), we display the asymptotic $\mathcal{N}_C$ versus the number of grid points N for square-lattice reconstruction grids as illustrated in Fig. 2. Here $\mathcal{N}_C$ is calculated with the flux data taken from all four sides. We find that $\mathcal{N}_C$ increases exponentially with the *linear* density of the reconstruction grid. The solid line in Fig. 5(a) is a fit to $\mathcal{N}_C=6$

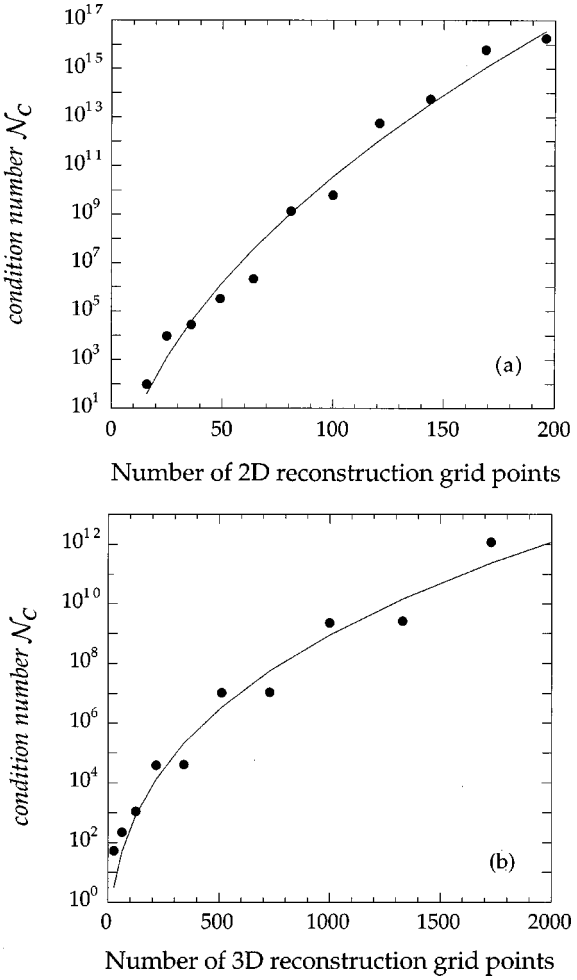

FIG. 5. Asymptotic condition number $\mathcal{N}_C$ versus the number of reconstruction grid points for a fixed area of a square turbid medium. $\mathcal{N}_C$ is obtained with the flux measurements made on all four sides of the medium. The solid line is a fit to $\mathcal{N}_C=6\times10^{-7}\exp(3.8N^{1/2})$, indicating the $\mathcal{N}_C$ increases exponentially with the linear density (instead of the aerial density) of the reconstruction grid. (b) Asymptotic condition number $\mathcal{N}_C$ versus the number of reconstruction grid points for a fixed volume of a cubic turbid medium. $\mathcal{N}_C$ is obtained with the diffuse photon flux measurements made on all four sides of the medium when their respective opposite side surfaces are uniformly illuminated. The solid line is a fit to $\mathcal{N}_C=7.2\times10^{-4}\exp(2.8N^{1/3})$, again indicating that $\mathcal{N}_C$ increases exponentially with the linear density (instead of the volume density) of the reconstruction grid.

$\times 10^{-7}\exp(3.8N^{1/2})$. This feature seems to be a general characteristic of a diffuse-photon computed tomography. In Fig. 5(b), we display the asymptotic condition number of matrices that relate a discrete set of optical absorption coefficients at N reconstruction grid points uniformly distributed in a cubic volume of a turbid medium to a sufficiently large set of flux measurements made at four side surfaces of the medium. In this three-dimensional (3D) case, we uniformly illuminate one side surface and detect the transmitted diffuse photons that emerge from the opposite side surface. Similar to the 2D case, $\mathcal{N}_C$ increases exponentially with the linear density of the reconstruction grid and the data are fit well to $\mathcal{N}_C = 7.2\times 10^{-4}\exp(2.8N^{1/3})$. This means that the quality or the signal-to-noise ratio of the image field deteriorates exponentially with the *linear* density of the reconstruction grid (instead of the aerial or volume density). It once again shows the ill conditioning of the kernel function $K(\mathbf{r}_s;\mathbf{r}')$ and the impossibility to achieve an arbitrarily high spatial resolution. We are presently investigating the physical or mathematical origins of the $N^{1/d}$ dependence of $\mathcal{N}_C$ with d being the dimensionality of the problem by analyzing the asymptotic behavior of the kernel function $K(\mathbf{r}_s;\mathbf{r}')$. It is noteworthy that to resolve heterogeneous structures with a uniform resolution of 0.3 cm throughout a 6 cm$\times$6 cm$\times$6 cm volume of a turbid medium, one would need to have $N=8000$ grid points. The corresponding $\mathcal{N}_C$ would be 1.5×10^{21}. In the next section, we will show that by using nonuniform reconstruction grids, one can reduce $\mathcal{N}_C$ dramatically and achieve the best overall spatial resolution in a diffuse photon tomography. We should note that using an *overly* fine reconstruction grid together with the regularization as described in Sec. II does not improve the *overall* image resolution. This is because the regularization acts as a low-pass ''spatial'' filter.

The exponential increase in $\mathcal{N}_C$ with the linear density of a reconstruction grid originates from the fact that the singular values of the kernel function $K(\mathbf{r}_s;\mathbf{r}')$ in Eq. (6) form an infinite sequence whose limit is zero. As the grid density increases, the matrix equation (7b) becomes a better approximation of the original integral equation [Eq. (6)]. As a result, the smallest singular values quickly approach zero, causing $\mathcal{N}_C$ to approach infinity.

Given the errors in the flux perturbation data and in $\mathbf{K}$, and given an acceptable signal-to-noise ratio of a computed tomographic image, one may determine the number of reconstruction grid points or the grid point density from Fig. 5(a) or 5(b). Such a procedure for determining the achievable image resolution is generally applicable to other forms of diffuse-photon computed tomography.

In the calculation that will be described in Sec. IV and in our recent experimental investigation, we find that a spatial resolution of 2–3 mm can be achieved with simulated and *experimental* flux perturbation data when imaging objects in a 6 cm$\times$6 cm$\times$6 cm volume of a turbid medium [22].

D. Benefit of using nonuniform reconstruction grids

In our investigation of the effect of regularization, we find that for a uniform reconstruction grid, the image resolution of objects far away from the boundary of a turbid medium is reduced or worsened the most, while that of objects near the boundary is much less affected. This hints that the diffuse photon flux emerging from a boundary surface contains more information about objects near the boundary than objects far away from it. It is then reasonable that the objects in the near boundary region should be imaged with a higher spatial resolution than those in the interior. This means that we should be able to achieve the best *overall* image resolution by using *nonuniform* reconstruction grids with higher density near the boundary and lower density in the middle of the medium. This proposition, if true, should be reflected by the dependence of $\mathcal{N}_C$ on where the high resolution is demanded. For example, we may expect $\mathcal{N}_C$ to increase slowly when we increase the grid density near the boundary and rapidly when we attempt to increase the density near the center of the medium. This is indeed the case.

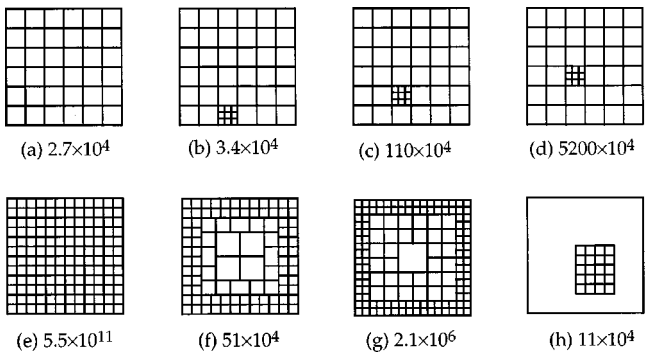

FIG. 6. Asymptotic condition number $\mathcal{N}_C$ versus uniform and nonuniform reconstruction grids for a fixed area of a square turbid medium.

In Fig. 6, we show a set of nonuniform reconstruction grids and two uniform grids with the corresponding asymptotic $\mathcal{N}_C$. When we *uniformly* increase the grid density by a factor of 2, i.e., from Fig. 6(a) directly to Fig. 6(e), $\mathcal{N}_C$ jumps from 2.7×10^4 to 5.5×10^{11} by more than 7 orders of magnitude. It is difficult from such a uniform density change to learn where we have paid the price for doubling the resolution. The answer lies in the results displayed from Fig. 6(b) to 6(c); in each case, the *linear* density of the grid points in a small, identically sized region is *tripled*, while the center of this small region is shifted progressively toward the interior. The total number of reconstruction grid points remains a constant. As we can see, $\mathcal{N}_C$ hardly changes when the high-density region is near the boundary: it quickly increases as the region moves towards the middle of the medium. It increases by more than 3 orders of magnitude as the high-density region is near the center of the medium. This result shows that the *overall image resolution* can be optimized by using a nonuniform reconstruction grid rather than a uniform grid. Figure 6(f) shows an example of such a *nonuniform reconstruction grid* in which we have quadrupled the density of the reconstruction grid everywhere near the boundary (occupying more than 50% of the total reconstruction area) while reducing the density near the center by 30%. Here $\mathcal{N}_C$ increases only by a factor of 20. Figure 6(g) is another example where the total number of the grid points remains the same as that in Fig. 6(e) except the grid density progressively decreases from the boundary to the center. $\mathcal{N}_C$ is only 2.1×10^6, a factor of 2×10^5 smaller than that for Fig. 6(e).

In practical imaging, an initial image reconstruction can be performed on a coarse, uniform grid. If the heterogeneity is found localized in one or a few small regions, one can perform the second reconstruction computation on a nonuniform grid with higher grid density only in the *reduced* regions where objects are located. In some cases, we can even use a truncated grid like the one shown in Fig. 6(h) if the optical absorption coefficient is constant outside the interrogated region. $\mathcal{N}_C$ increases only slightly from that for Fig. 6(a) even when the grid density near the center of the medium is quadrupled.

IV. DIFFUSE-PHOTON COMPUTED TOMOGRAPHY IN THREE DIMENSIONS

To test some of the findings in the preceding sections, we have performed a numerical study in which we image absorptive objects in a 3D volume of a turbid medium. For convenience rather than necessity, we assume that the turbid medium under consideration is homogeneous and *nonabsorbing*, and it has a reduced scattering coefficient $\mu_s' = 1/l_{\rm tr} = 17\,{\rm cm}^{-1}$. It is contained in a square column that is infinitely extended along z axis and has a width $L = 6$ cm along x and y axes. The objects to be imaged consist of three letter-shaped objects ''D,'' ''C,'' and ''U.'' They are 1 cm in overall size and have a width of 0.24 cm. They are distributed in the medium over a range of 6 cm along z axis. The planes of these letter-shaped objects are parallel to the x-y plane. We choose the origin of the z axis so that the objects are confined in a volume section between $z = 0$ and 6 cm. The centers of D, C, and U are at $\{x', y', z'\} = \{2.88\,{\rm cm}, 3.12\,{\rm cm}, 4.20\,{\rm cm}\}$, $\{4.08\,{\rm cm}, 1.68\,{\rm cm}, 2.28\,{\rm cm}\}$, and $\{1.68\,{\rm cm}, 4.08\,{\rm cm}, 2.28\,{\rm cm}\}$, respectively. Our objective is to determine the achievable spatial resolution of our tomographic algorithm. For this purpose we choose the absorption coefficients of these letter-shaped objects to be $\mu_a \equiv 1.3\,{\rm cm}^{-1}$.

In our calculation, we uniformly ''illuminate'' one side surface of the medium. Our detection strategy is to only ''measure'' the diffuse photon flux emerging from a 6 cm×6 cm section on the opposite surface between $z = 0$ and 6 cm or the surface of the volume section between $z = 0$ and 6 cm. In Fig. 7 we show the sketch of the illumination-detection arrangement. The 6 cm×6 cm surface section is uniformly divided into $23 \times 35 = 805$ pixels that are of rectangular shape with the long side along the z axis. To obtain the simulated flux perturbation data for image reconstruction, we solve the forward problem and evaluate the flux emerging from the centers of the 805 pixels. We first calculate the flux in the absence of the objects and then the flux in the presence of the objects, and finally we take the difference between the two as the flux perturbation data. We repeat the illumination-detection sequence for each of the other three surfaces and obtain a total of $M = 805 \times 4 = 3220$ flux perturbation data. In Fig. 8, we display the calculated flux perturbation from the four surface sections when the corresponding opposite surface is uniformly illuminated. The displayed data are normalized by the flux taken in the absence of the objects. It is obvious that there are objects inside the medium. The question is, can one pin down the center locations of the objects and resolve their structures in original details?

To examine whether our tomographic algorithm enables

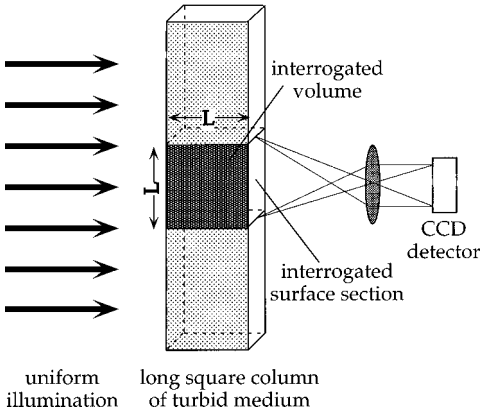

FIG. 7. Sketch of an illumination-detection arrangement for a continuous-wave diffuse photon computed tomography. The turbid medium is a long column with a square cross section of 6 cm ×6 cm. One face of the medium is uniformly illuminated with a continuous-wave light. The normal component of the diffuse photon flux that emerges from a 6 cm×6 cm surface section on the opposite side of the medium is detected with an imaging optics and a charge coupled device (CCD) detector. Four such 6 cm×6 cm surface sections enclose a 6 cm×6 cm×6 cm volume section that is to be imaged.

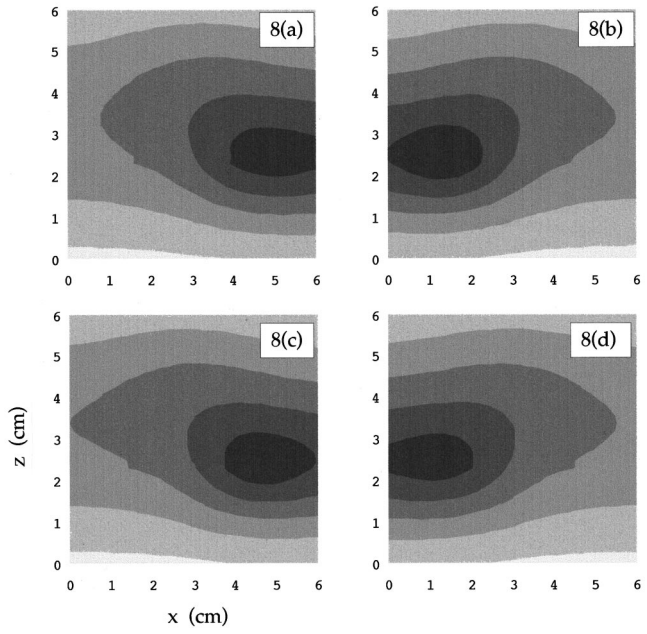

FIG. 8. Contour plots of the perturbed flux $J_n = J_{n0} + j_n$ normalized by the unperturbed flux J_{n0} from four 6 cm×6 cm surface sections of a 6 cm×6 cm×6 cm volume section that contains three letter-shaped objects. The volume section is a part of a long, square column of turbid medium. The difference between two successive contours is 0.1. (a) The normalized diffuse photon flux emerging from the surface section at $y = 0$ when the opposite surface at $y = 6$ cm is illuminated. (b) The normalized diffuse photon flux emerging from the surface section at $x = 6$ cm when the opposite face at $x = 0$ is illuminated. (c) The normalized diffuse photon flux emerging from the surface section at $y = 6$ cm when the opposite face at $y = 0$ is illuminated. (d) The normalized diffuse photon flux emerging from the surface section at $x = 0$ when the opposite face at $x = 6$ cm is illuminated.

us to achieve high spatial resolution, we adopt a nonuniform grid as illustrated by Fig. 6(h). Knowing that the objects are localized only in three $(1.2\ \mathrm{cm})^3$ volume sections, it is only necessary for us to image the distribution of optical absorption coefficients in these three regions. We do so by discretizing the three $(1.2\ \mathrm{cm})^3$ volume sections that contain the three letter-shaped objects, each into $6\times6\times6=216$ cubic *voxels*. The region containing the object D starts at $\{x', y', z'\}=\{2.5\ \mathrm{cm}, 2.5\ \mathrm{cm}, 3.72\ \mathrm{cm}\}$ and ends at {3.7 cm, 3.7cm, 4.92 cm}. The region containing the object C starts at $\{x', y', z'\}=\{2.4\ \mathrm{cm}, 1.2\ \mathrm{cm}, 1.8\ \mathrm{cm}\}$ and ends at {3.6 cm, 2.4 cm, 3.0 cm}. The region containing the object U starts at $\{x', y', z'\}=\{1.2\ \mathrm{cm}, 2.4\ \mathrm{cm}, 1.8\ \mathrm{cm}\}$ and ends at {2.4 cm, 3.6 cm, 3.0 cm}. From the three regions of interest, we have total $N=648$ optical absorption coefficients to determine from the flux perturbation measurements. It is easy to find the Green function $G(x,y,z;x',y',z')$ and the unperturbed diffuse photon density $\Phi_0(x,y)$ in the present geometry. From an integral equation similar to Eq. (5), we arrive at a 3220×648 matrix **K** that relates 648 optical absorption coefficients to 3220 flux perturbation data. We compute the optical absorption coefficients $\tilde{\mu}_a$ by performing an inversion of **K** with the method of SVD.

The condition number of the 3220×648 matrix **K** is found to be $\mathcal{N}_C=4\times10^{10}$. If 648 is uniformly distributed over the $6\ \mathrm{cm}\times6\ \mathrm{cm}\times6\ \mathrm{cm}$ volume instead of only over the three localized regions, $\mathcal{N}_C$ is reduced to 2×10^7 according to Fig. 5(b). To see how well the distribution of optical absorption coefficients *can* be resolved and how the round-off errors in computing the flux perturbation data and the matrix **K** affect the image quality, we performed two image calculations: one is done with *single-machine precision* that nominally has a fractional accuracy of 10^{-8} in representing the floating-point numbers; the other is done with *double-machine precision* that nominally has a fractional accuracy of 10^{-16}.

In Figs. 9 and 10, we display 2D contour plots of the *reconstructed* optical absorption coefficients in the *x-y* plane that are obtained with double-machine precision. Figure 9 shows three consecutive image planes that are separated along the *z* axis by 0.24 cm from $z=3.96$ to 4.44 cm, Figure 10 shows three consecutive *x-y* planes that are also separated along the *z* axis by 0.24 cm from $z=2.04$ to 2.52 cm. The best reconstruction is obtained *directly* from Eq. (8) without any regularization on the matrix **K** or **W**. The distribution of the optical absorption coefficients that characterizes all three letter-shaped objects is *completely* restored. In fact, the reconstructed values agree with the set values of $\mu_a \equiv 1.3\ \mathrm{cm}^{-1}$ within a few parts in 10^6. At grid points where optical absorption coefficients are set to zero in the forward problem, the reconstructed values are in the range of $10^{-6}\ \mathrm{cm}^{-1}$ or a few millionths of $\mu_a \equiv 1.3\ \mathrm{cm}^{-1}$.

In Figs. 11 and 12, we display 2D contour plots of the reconstructed optical absorption coefficients obtained with the single-machine precision. In this case we have effectively added accumulative machine round-off errors to the calculation. According to Golub and van Loan, the error in the reconstructed image has a contribution that may be as large as the accumulative round-off errors multiplied by the condition number. We find it to be qualitatively the case here. If the reconstruction computation is done without any regularization, the reconstructed image is dominated by artifacts produced by the round-off errors. When we apply the zeroth-order regularization to the inversion by using Eqs. (10) and (11), the original distribution of the optical extinction coefficient is partially restored. The best images as shown in Figs. 11 and 12 are obtained with a regularization parameter

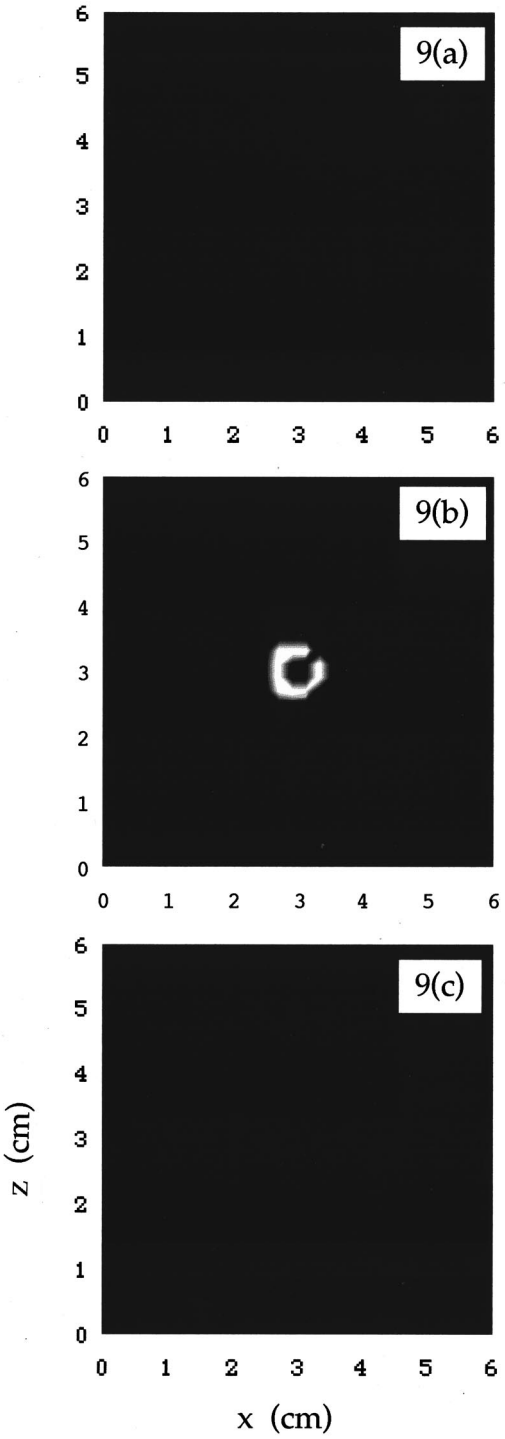

FIG. 9. Two-dimensional contour plots of the reconstructed optical extinction coefficients in three *x-y* planes from $z=3.96$ to 4.44 cm. The planes are separated by 0.24 cm. The difference in optical extinction coefficients between two successive contours is 0.26 cm^{-1} or 1/5 of $\mu_a \equiv 1.3\ \mathrm{cm}^{-1}$. The image reconstruction calculation is performed with double-machine precision. (a) $z=3.96$ cm, (b) $z=4.20$ cm. (c) $z=4.44$ cm.

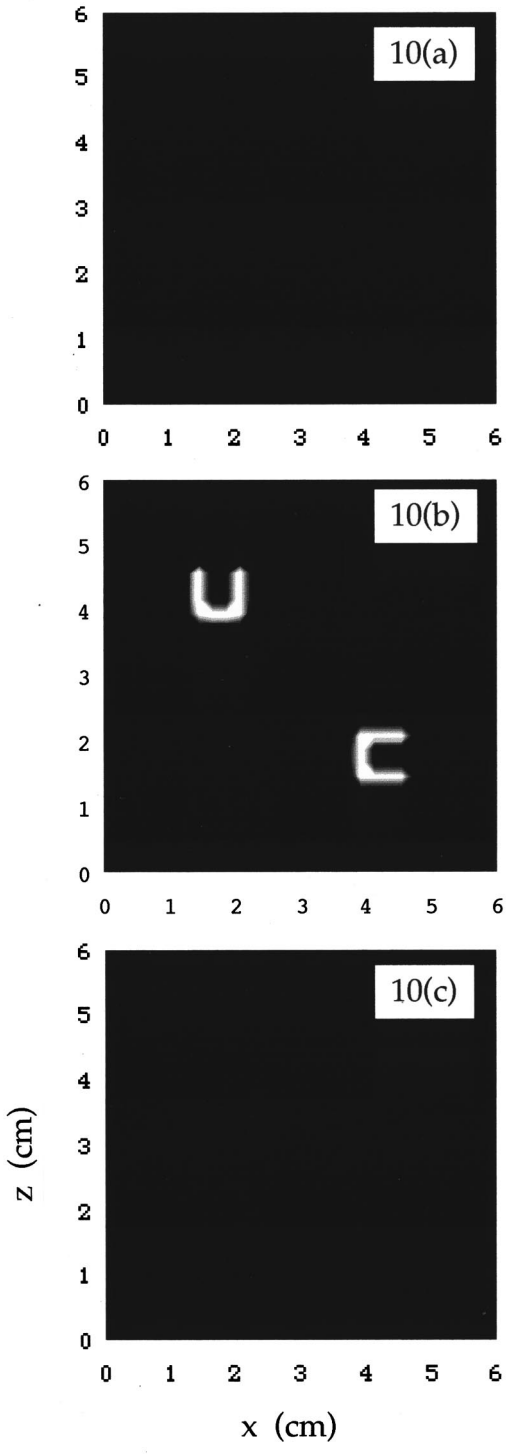

FIG. 10. Two-dimensional contour plots of the reconstructed optical extinction coefficients in three x-y planes from $z=2.04$ to 2.52 cm. The planes are separated by 0.24 cm. The difference in optical extinction coefficients between two successive contours is 0.26 cm^{-1} or 1/5 of $\mu_a \equiv 1.3\,cm^{-1}$. The image reconstruction calculation is performed with *double-machine precision*. (a) $z=2.04$ cm. (b) $z=2.28$ cm, (c) $z=2.52$ cm.

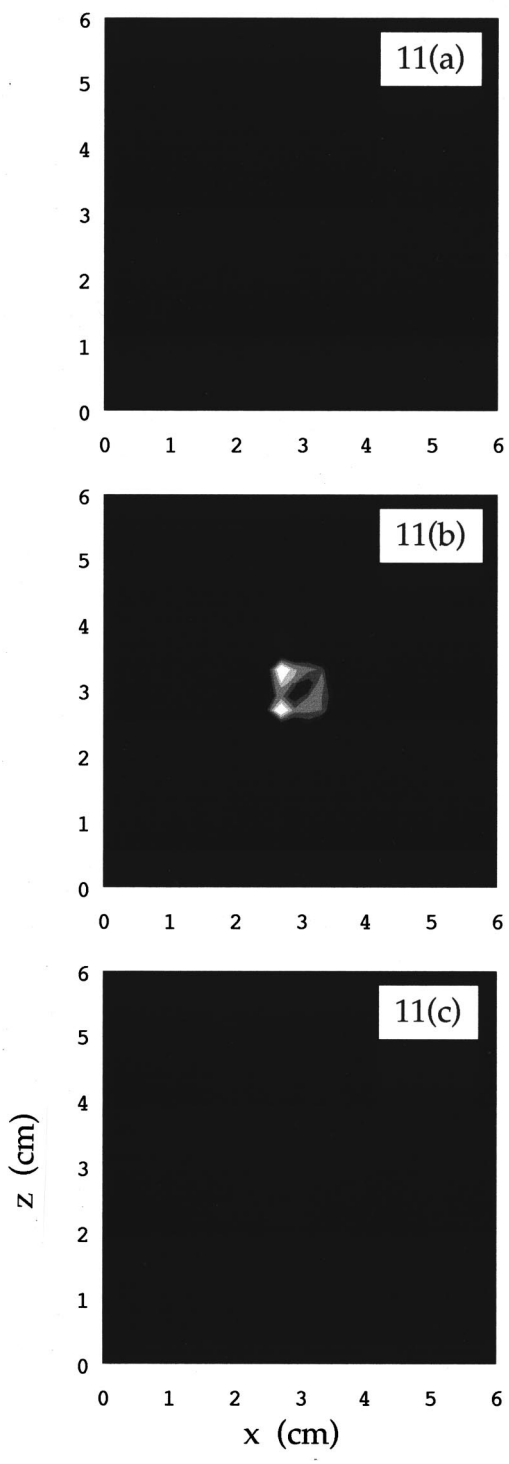

FIG. 11. Two-dimensional contour plots of the reconstructed optical extinction coefficients in three x-y planes from $z=3.96$ to 4.44 cm. The planes are separated by 0.24 cm. The difference in optical extinction coefficients between two successive contours is 0.26 cm^{-1} or 1/5 of $\mu_a \equiv 1.3\,cm^{-1}$. The image calculation is performed with *single-machine precision*. (a) $z=3.96$ cm. (b) $z=4.20$ cm. (c) $z=4.44$ cm.

$\alpha = 7 \times 10^{-6}$. The position and shape of all three objects are again reproduced. The values of μ_a are reproduced within 10% of the original values for letters C and U, and only within 40% of the original value for letter D. Most noticeably, the spatial resolution is deteriorated as a result of the regularization. The broadening of the image are less than 0.24 cm for objects C and U, both of which are closer to the boundary of the medium. For object D, which is located in the middle of the investigated volume section, the broadening increases to 0.5 cm. This shows that the regularization

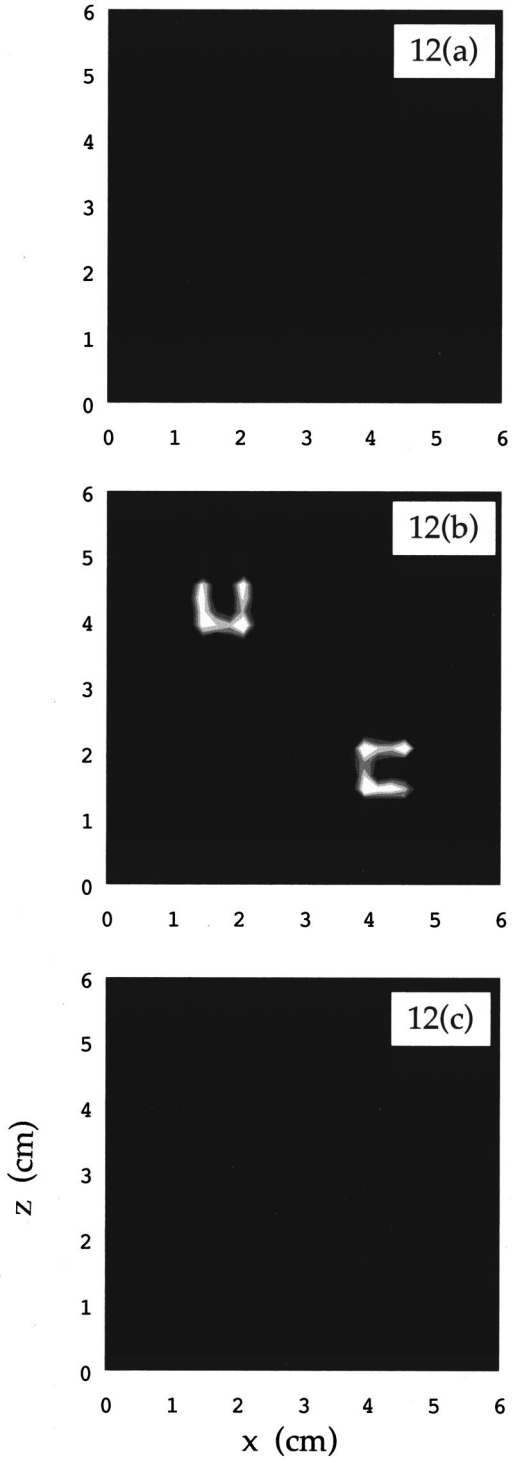

FIG. 12. Two-dimensional contour plots of the reconstructed optical extinction coefficients in three x-y planes from $z=2.04$ to 2.52 cm. The planes are separated by 0.24 cm. The difference in optical extinction coefficients between two successive contours is 0.26 cm^{-1} or 1/5 of $\mu_a \equiv 1.3\,cm^{-1}$. The image calculation is performed with *single-machine precision*. (a) $z=2.04$ cm. (b) $z=2.28$ cm. (c) $z=2.52$ cm.

has the largest effect on the image resolution of objects in the interior of the medium and has the least effect on that of objects near the boundary.

We have recently performed an experiment to test our imaging algorithm with *experimentally measured* flux perturbation data [22]. In the experiment we imaged a 30-mm-long and 2.5-mm-diam capillary tube in a column of a turbid medium. The wall thickness of the capillary tube is 0.4 mm. The column has a square cross section of 5 cm×5 cm and is filled with a 4% Intralipid emulsion (from Kabi Pharmacia, Clayton, NC) as the turbid medium. The reduced scattering coefficient of the medium is measured to be $\mu_s' = 27\,cm^{-1}$ at the He-Ne wavelength of 633 nm. As an absorbing object, the capillary tube is filled with the same Intralipid emulsion except we have added India Ink dye so that the optical absorption coefficient of the Intralipid emulsion in the tube is $\mu_a = 0.1\,cm^{-1}$. This corresponds to $\mu_a/\mu_s' = 0.0037$, comparable to $\mu_a/\mu_s' = 0.0024$ in normal human breast tissue at 780 nm [28]. Using *experimentally* measured flux and the strategy described in this section, we were able to image the capillary tube with a spatial resolution of 2.5 mm.

Our numerical calculation, supported by the results of our recent experiment, shows that by properly choosing the illumination-detection scheme and the reconstruction grid it is indeed *feasible* to image objects in a 6 cm×6 cm×6 cm volume of a turbid media with a spatial resolution as high as 2.4 mm.

Finally, we remark on the issue of the uniqueness of reconstructed images as investigated in the present numerical study and in the experimental study to be reported separately [22]. Recently, Hoenders showed that, rigorously speaking, the reconstructed image is not unique in any form of optical tomography that is based on diffuse photon flux measurements at the surface of an interrogated turbid medium [29]. There exists (at least) a class of object distributions that generate no detectable perturbation to the diffuse photon flux at the surface. This may seem in contradiction to the fact that many groups, including us, have already obtained reasonable images of simple objects using various forms of diffuse photon optical tomography experimentally as well as numerically. The answer lies in the fact that the uniqueness of a reconstructed image is determined by the property of the kernel function $K(\mathbf{r}_s;\mathbf{r}')$ in Eq. (6) and in the discretized form by the condition number of the matrix **K** as defined in Sec. II.

As correctly pointed out by Hoenders [29], a *continuous* distribution of optical absorption coefficient $\mu_a(\mathbf{r}')$ that characterizes an object distribution in a turbid medium *cannot be uniquely determined in its infinite detail* through Eq. (6) even with full knowledge of the diffuse photon flux $j_n(\mathbf{r}_s)$ that emerges from the surface of the medium. In the framework of the present study, the nonuniqueness of *continuously* reconstructed images or $\mu_a(\mathbf{r}')$ is reflected by the fact that when the reconstruction grid is infinitely fine, the condition number of the resultant matrix **K** equals to infinity. As clearly shown in Fig. 5, the condition number diverges exponentially as the linear density of the reconstruction grid increases. It means that in the continuous limit there are infinite solutions that solve Eq. (6). As also correctly demonstrated by many groups, including us, a finite, discrete distribution of optical absorption coefficient $\tilde{\mu}_a$ that *approximately* characterizes an object distribution *can be uniquely determined* from a finite set of diffuse photon flux $\tilde{j}_n$ measured at the surface of a turbid medium. This is re-

flected by the fact that the condition number of a finite matrix **K** is finite.

By approximating a continuous distribution of objects with a finite, discrete distribution, one automatically rejects those solutions (infinite in number) of Eq. (6) that have spatial frequencies larger than the inverse of the grid point separation of the discrete distribution. The relevant questions to ask are (1) whether such a discrete distribution of optical absorption coefficient $\tilde{\mu}_a$ has an adequate spatial resolution and sensitivity for the realistic purpose of the tomography and (2) whether the discretization scheme and the choice of illumination-detection combinations can be optimized to give the best overall resolution and sensitivity. In our present numerical study, we have precisely addressed these two issues. For potential applications in early breast cancer detection and optically guided biopsy of breast tumors, a spatial resolution of 2–3 mm would make the optical tomopgraphic imaging technique competitive to x-ray-based imaging techniques. We have demonstrated here that such a resolution is indeed achievable and one can use the condition number as the measure of the uniqueness and the stability of a reconstructed image against the errors in model description (including computational error) and in diffuse photon flux measurements. Most importantly, we have also shown that *experimentally measured* (rather than computer-simulated) diffuse photon flux has a sufficiently high signal-to-noise ratio to yield stable images of objects in a turbid medium with a spatial resolution of 2.4 mm and a sensitivity adequate for breast cancer detection [22].

V. CONCLUSION

We have shown here a perturbation analysis that offers a book-keeping method for evaluating a diffuse-photon computed tomography of a turbid medium. The tomography is based upon the measurement of the diffusely scattered photons that emerge from the surface of the medium. Such an analysis enables us to quantitatively compare the effectiveness of various illumination-detection arrangements and the reconstruction algorithms (including reconstruction grid selection). Since the condition number ($\mathcal{N}_C$) of the matrix **K** (obtained from a perturbation analysis) is in essence the amplification factor of the errors in the surface flux measurement and the model description of the diffuse photons, and in the image reconstruction computation, we find that the optimization of a diffuse-photon computed tomography is achievable through a systematic minimization of $\mathcal{N}_C$. Our main findings are the following: (1) it is *necessary* and *sufficient* to make the number of surface flux measurements be twice as many as the number of image reconstruction grid points; (2) multiple illumination-detection arrangements are necessary for minimizing the condition number and the minimization can be quantified; (3) given a required signal-to-noise ratio for the image, one can achieve the best overall image resolution throughout the interrogated medium by using nonuniform reconstruction grids; and (4) the *experimental* flux perturbation data have a sufficiently high signal-to-noise ratio to enable a continuous-wave diffuse photon tomography of objects in a 6 cm×6 cm×6 cm turbid medium with a spatial resolution of 2.4 mm.

ACKNOWLEDGMENT

This work is supported by the DOE Center of Excellence for Laser Application in Medicine under Grant No. DEFG0398ER62576.

[1] *Medical Optical Tomography: Functional Imaging and Monitoring*, edited by G. Müller, B. Chance, R. Alfano, S. Arridge, J. Beuthan, E. Gratton, M. Kaschke, B. Masters, S. Svanberg, and P. Vander Zee (SPIE, Bellmingham, WA, 1993).

[2] *Diffuse Photons in Turbid Media*, edited by B. Tromberg, A. Yodh, E. Sevick, and D. Pines [Appl. Opt. **36,** 9 (1997)].

[3] *Diffuse Photons in Turbid Media*, edited by B. Tromberg, A. Yodh, E. Sevick, and D. Pines [J. Opt. Soc. Am. A **14,** 136 (1997)].

[4] R. J. Bartrum and H. C. Crow, Am. J. Roentgenol. **142**, 409 (1984); E. A. Sickles, *ibid.* **142**, 841 (1984); G. E. Geslien, J. R. Fisher, and C. DeLaney, *ibid.* **144**, 619 (1985); J. J. Gisvold, L. R. Brown, R. G. Swee, D. J. Raygor, N. Dickerson, and M. K. Ranfranz, *ibid.* **147**, 191 (1986); E. A. Sickles, in *Recent Results in Cancer Research*, edited by S. Brünner and B. Langfeldt (Springer-Verlag, New York, 1990), Vol. 119, p. 127.

[5] A. Knüttel, J. M. Schmitt, and J. R. Knutson, Appl. Opt. **32**, 381 (1993); A. Knüttel, J. M. Schmitt, R. Barnes, and J. R. Knutson, Rev. Sci. Instrum. **64**, 638 (1993).

[6] B. Chance, K. Kang, L. He, J. Weng, and E. Sevick, Proc. Natl. Acad. Sci. USA **90**, 3423 (1993).

[7] M. A. O'Leary, D. A. Boas, B. Chance, and A. G. Yodh, Opt. Lett. **20**, 426 (1995).

[8] M. A. O'Leary, D. A. Baos, X. D. Li, B. Chance, and A. G. Yodh, Opt. Lett. **21**, 158 (1997).

[9] X. D. Li, T. Durduran, A. G. Yodh, B. Chance, and D. N. Pattanayak, Opt. Lett. **22**, 573 (1997).

[10] S. Fantini, M. Franceschini, G. Gaida, E. Gratton, H. Jess, W. W. Mantulin, K. T. Moesta, P. Schlag, and M. Kaschke, Med. Phys. **23**, 149 (1996), and references therein; M. A. Franceschini, K. T. Moesta, S. Fantini, G. Gaida, E. Gratton, H. Jess, W. W. Mantulin, M. Seeber, P. M. Schlag, and M. Kaschke, Proc. Natl. Acad. Sci. USA **94**, 6468 (1997).

[11] D. Y. Paithankar, A. U. Chen, B. W. Pogue, M. S. Patterson, and E. M. Sevick-Muraca, Appl. Opt. **36**, 2260 (1997).

[12] H. Jiang, K. D. Paulsen, U. L. Osterberg, and M. S. Patterson, Appl. Opt. **36**, 52 (1997); K. D. Paulsen and H. Jiang, Med. Phys. **22**, 691 (1997).

[13] P. N. den Outer, Th. M. Nieuwenhuizen, and A. Lagendijk, J. Opt. Soc. Am. A **10**, 1209 (1993).

[14] R. L. Barbour, H. L. Graber, Y. Wang, Jeng-Hwa Chang, and R. Aronson, in *Medical Optical Tomography: Functional Imaging and Monitoring*, edited by G. Müller, B. Chance, R. Alfano, S. Arridge, J. Beuthan, E. Gratton, M. Kaschke, B. Masters, S. Svanberg, and P. Vander Zee (SPIE, Bellingham, WA, 1993), p. 87.

[15] X. D. Zhu, Sung-po Wei, and Xiaowen Guo, J. Opt. Soc. Am. A **14**, 300 (1997).
[16] Shechao Feng, Fan-An Zeng, and B. Chance, Appl. Opt. **34**, 3826 (1995).
[17] X. D. Zhu, Sung-po Wei, S. C. Feng, and B. Chance, J. Opt. Soc. Am. A **13**, 494 (1996).
[18] Th. M. Nieuwenhuizen and M. C. W. van Rossum, Phys. Lett. A **177**, 102 (1993).
[19] G. H. Golub and C. F. Van Loan, *Matrix Computations* (Johns Hopkins University Press, Baltimore, 1983), p. 16.
[20] W. H. Press, B. P. Flannery, S. A. Teukolsky, and W. T. Vetterling, *Numerical Recipes in FORTRAN: The Art of Scientific Computing*, 2nd ed. (Cambridge University Press, New York, 1992), Chap. 2.
[21] G. H. Golub and C. F. Van Loan, *Matrix Computations* (Johns Hopkins University Press, Baltimore, 1983), p. 24.
[22] Sung-po Wei, Tuo Zhu, Huiming Zhu, and X. D. Zhu (unpublished).
[23] See, for instance, Kenneth M. Case and Paul F. Zweifel, *Linear Transport Theory* (Addison-Wesley, Palo Alto, CA, 1967).
[24] F. R. deHoog, in *The Application and Numerical Solution of Integral Equations*, edited by R. S. Andersson, F. R. deHoog, and M. A. Lukas (Sijthoff & Noordhoff, Germantown, MD, 1980), p. 119.
[25] L. M. Delves and J. L. Mohamed, *Computational Methods for Integral Equations* (Cambridge University Press, Cambridge, England, 1985), p. 307.
[26] A. N. Tikhonov, Sov. Mat. Dokl. **4**, 1624 (1963); A. N. Tikhonov and V. Y. Arsenin, *Solutions of Ill-Posed Problems* (Wiley, New York, 1977).
[27] P. C. Hansen, SIAM Rev. **34**, 561 (1992).
[28] A. Yodh and B. Chance, Phys. Today **48**(3), 34 (1995).
[29] B. J. Hoenders, J. Opt. Soc. Am. A **14**, 262 (1997).